Giant enhancement of the in-plane critical field for thin Al films via proximity coupling to a topological insulator

Zhu Lin,[1] Zhilin Li,[2] Haoyun Deng,[1] Tianhan Liu,[1] Gang Shi,[2] Nicholas Bonesteel,[1,3] Pedro Schlottmann,[1] Yongqing Li,[2,4] and Peng Xiong[1,*]

[1]*Department of Physics, Florida State University, Tallahassee, Florida 32306, USA*
[2]*Beijing National Laboratory for Condensed Matter Physics, Institute of Physics, Chinese Academy of Sciences, Beijing 100190, China*
[3]*National High Magnetic Field Laboratory, Tallahassee, Florida 32310, USA*
[4]*School of Physical Sciences, University of Chinese Academy of Sciences, Beijing 100049, China; Songshan Lake Materials Laboratory, Dongguan, Guangdong 523808, China; and CAS Center for Excellence in Topological Quantum Computation, University of Chinese Academy of Sciences, Beijing 100190, China*

(Received 8 July 2020; accepted 28 September 2020; published 20 October 2020)

A topological superconducting state can be induced in the surface state of a topological insulator (TI) by way of proximity coupling to a conventional *s*-wave superconductor (*s*-SC). Planar *s*-SC/TI junction structures were proposed as a scalable platform for controlled generation and manipulation of Majorana zero mode (MZM), which holds intriguing promise for fault-tolerant quantum computing. Despite intensive research efforts, the presence of MZM has not been definitively demonstrated in *s*-SC/TI/*s*-SC lateral junctions. A key factor is a lack of direct measurement and quantitative understanding of the proximity coupling between the *s*-SC and TI. Here we report evidence for strong superconducting proximity effect between a three-dimensional strong TI and Al, a conventional *s*-SC with minimal intrinsic spin-orbit coupling, in the form of pronounced enhancement of the in-plane critical field ($H_{c||}$) of the thin Al. Specifically, the $H_{c||}$ of a 6-nm-thick Al film deposited on a TI is found to be 2.7 times its Pauli limit and about three times that of a simultaneously deposited reference film on Si/SiO_2. The analysis of the $H_{c||}$ enhancement within the Maki theory indicates significant induced spin-orbit interaction in the Al due to electronic coupling to the TI. Our results revealed a pathway for producing SC/TI devices of high interfacial electrical transparency conducive for MZM generation and manipulation.

DOI: 10.1103/PhysRevB.102.144518

I. INTRODUCTION

Electronic excitations obeying non-Abelian statistics are of pertinent interest due to their potential in fault-tolerant quantum computation [1,2]. One physical system in which such non-Abelian anyons may emerge, in the form of Majorana zero mode (MZM), is the $p_x + ip_y$ spinless superconducting state [1,2]. Naturally occurring *p*-wave superconductors are rare and fragile, susceptible to even a minute amount of disorder [3]. Topological superconductivity may materialize on the surfaces of bulk superconductors which also possess topological surface states [4–6]. However, the bulk superconductivity presents a formidable obstacle for patterning the superconducting surface, which is necessary for controlled MZM generation and manipulation. A more robust and versatile platform for the generation and manipulation of the MZMs is the artificial topological superconducting state at the surface of a semiconductor with strong spin-orbit (SO) interaction and large Landé *g* factor [7] or a three-dimensional (3D) strong topological insulator (TI) [8], induced via proximity coupling to a conventional *s*-wave superconductor (*s*-SC). In the former, there is compelling conductance spectroscopy evidence for the existence of a MZM at the end of an Al-coated InSb or InAs nanowire [9,10]. However, a carefully oriented Zeeman-splitting magnetic field is required for the materialization of the MZM [7] and the nanowire-based device structure continues to present challenges for manipulation of the MZMs necessary for realizing qubit formation and operation. In an *s*-SC/TI heterostructure, clear signatures of MZMs at the superconducting vortex cores were identified in spin-polarized Andreev reflection spectroscopy [11]. In this platform, Fu and Kane [8] had proposed a set of schemes for MZM generation, fusion, and braiding based on *planar* superconducting junctions on a TI. Besides being amenable to upscaling, a particularly attractive characteristic of the schemes is their reliance on the control of the superconducting phases across the junctions, without the need for a large magnetic field.

As a first step in the implementation of the Fu-Kane schemes, there have been extensive experimental efforts aimed at validating the presence of MZMs in the simplest devices, the S/TI/S line junctions, via measurements of both conductance spectroscopy [12–15] and the Josephson effect [16–22]. Despite these targeted activities, the very existence of MZMs in S/TI/S line junctions remains an open issue. Many factors contribute to the ambiguities and difficulties in the interpretation of the experimental results. One key factor is the uncertainty or lack of direct measurement of the superconducting proximity effect between the TI and SC in such devices. The topological superconducting state in *s*-SC/TI heterostructures is supposed to originate from electronic coupling between the *s*-wave superconductivity and

*pxiong@fsu.edu

the spin-helical surface state of the TI [8]. The presence of the *s*-SC in the heterostructure precludes measurement of the proximity-induced superconductivity in the TI surface state via transport or thermodynamic measurements. Moreover, because the SC/TI interface is embedded in the heterostructure, even a local probe such as scanning probe spectroscopy cannot be applied directly to the interface. For instance, the scanning Andreev reflection spectroscopy on Bi_2Se_3 epitaxially grown on $NbSe_2$ had to be performed on its top surface, where the proximity coupling to the SC goes through the bottom surface and bulk of the TI [11], which significantly complicated the interpretation.

In this work, we probe the proximity coupling between a 3D strong TI, $(Bi_{0.5}Sb_{0.5})_2TeSe_2$ (BSTS), and an *s*-SC, Al, by measuring the in-plane critical field ($H_{c||}$) of the thin Al films deposited on the TI. Al (and Be) is considered a model spin-singlet Bardeen-Cooper-Schrieffer (BCS) SC because of its minimal intrinsic SO interaction [23–28]: In the presence of an in-plane magnetic field, the single-particle density of states of thin superconducting Al (Be) films are shown to exhibit clean Zeeman splitting, and their $H_{c||}$ are well described by the theory of Clogston [29] and Chandrasekhar [30] (the Pauli limit). The introduction of SO scattering into thin Al (Be) films, typically via deposition of a small amount of heavy metal elements on top, leads to spin mixing [23,27] and large enhancement of $H_{c||}$ [23,27]. A full description of H_c, incorporating the effects of Zeeman energy, orbital depairing, and SO interaction, can be obtained based on the Maki theory [31,32]. For a thin *s*-SC film in an in-plane field, the orbital depairing is minimized and a measurement of H_c can be used to evaluate the SO scattering rate. Our experiments reveal a giant enhancement of $H_{c||}$ beyond the Pauli limit for thin Al films deposited on BSTS, which constitutes direct evidence for significant SO interaction induced in Al via proximity coupling to the TI.

II. EXPERIMENTS AND RESULTS

Figures 1(a) and 1(b) show schematic diagrams of an Al/BSTS sample and measurement configuration. Figure 1(c) is an optical micrograph of a BSTS flake with Cr/Au contacts and an Al Hall bar deposited via thermal evaporation. The experimental details are presented in the Methods section. Briefly, the BSTS crystals were grown using a self-flux method. A critical step in the crystal growth is a month-long controlled cool-down process, resulting in high-quality BSTS crystals of dimensions as large as centimeters and insulating bulk as grown. For device fabrication, a flake of BSTS was exfoliated from a crystal and placed on a Si/SiO_2 substrate. The typical areas of the flake were 1 mm^2 and thickness $\sim$100 μm. The insulating bulk and surface state-dominated transport at low temperatures in such samples are evidenced by the $R(T)$ of such a BSTS flake, as described in detail in Supplemental Material S1 [33]; also see Ref. [34]. The large size of the flake was necessary to accommodate the subsequent metal evaporations through *mechanical shadow masks*. First, Al was deposited on the BSTS via thermal evaporation as a Hall bar pattern [Fig. 1(c)]. The exposure of the BSTS flake to ambient air before the Al deposition (e.g., for the setup of the shadow mask) was typically limited to a few minutes. The

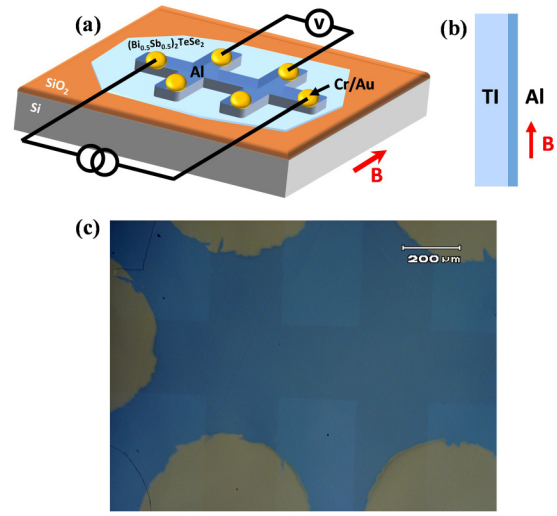

FIG. 1. Schematics and optical micrograph of the Al/TI device structure and measurement scheme. (a) Schematics of the Hall-bar device and the measurement configuration. (b) Schematic representation of the magnetic field oriented in the film plane. (c) Optical micrograph of a device with a 6-nm Al film on a $(Bi_{0.5}Sb_{0.5})_2TeSe_2$ flake. The BSTS flake was mechanically exfoliated from a crystal and placed on a Si/SiO_2 substrate.

use of a shadow mask, instead of lithography, not only greatly reduced the air exposure time, but more importantly, *eliminated* any exposure to solvent, UV, or electron beam. Once the Al/BSTS interface was formed, it was found to be stable in ambient air for days. Cr/Au contacts were then deposited via a second shadowed evaporation. Despite the stability of the Al/BSTS interface, we always tried to cool down the sample in a cryostat as quickly as possible. For every Al/BSTS sample, a reference sample of Al was made simultaneously under identical conditions on a Si/SiO_2 substrate. The temperature (T) and magnetic field (H) dependences of the resistance for the two samples were measured simultaneously in an Oxford ^{3}He system. For accurate determination of the $H_{c||}$, the field alignment with the film plane is critical. In our experiments, the alignment was optimized by fine-tuning the sample stage *in situ* (for details, see Supplemental Material S2 [33]; also see Ref. [35]). Figures 2(a)–2(f) show the normalized $R(T)$ in zero field and $R(H_{||})$ at $T = 0.40$ K for three sets of Al films ($t = 15$, 9.0, and 6.0 nm) on BSTS (red) and Si/SiO_2 (black). In the data presented below, the transition temperatures (T_C) and the critical field were defined by the temperature and field, respectively, corresponding to the midpoint of the resistive transitions. With decreasing t, the zero-field T_C of the reference samples on Si/SiO_2 show a gradual increase from 1.52 to 1.87 K, consistent with previous reports [23]. The T_C of the respective Al films on BSTS are similar to or slightly higher than those of the reference samples. In contrast, with decreasing t, $H_{c||}$ of the Al films on BSTS show increasingly large enhancement beyond $H_{c||}$ of the reference samples. As is evident in Fig. 2(f), at $T = 0.40$ K, the 6-nm Al film on BSTS remains superconducting at $H_{||} = 8$ T, while $H_{c||}$ of the reference sample is 3.2 T.

The different $H_{c||}$ of the two types of Al films and their evolution with the Al thickness are plotted in Fig. 3(a). In

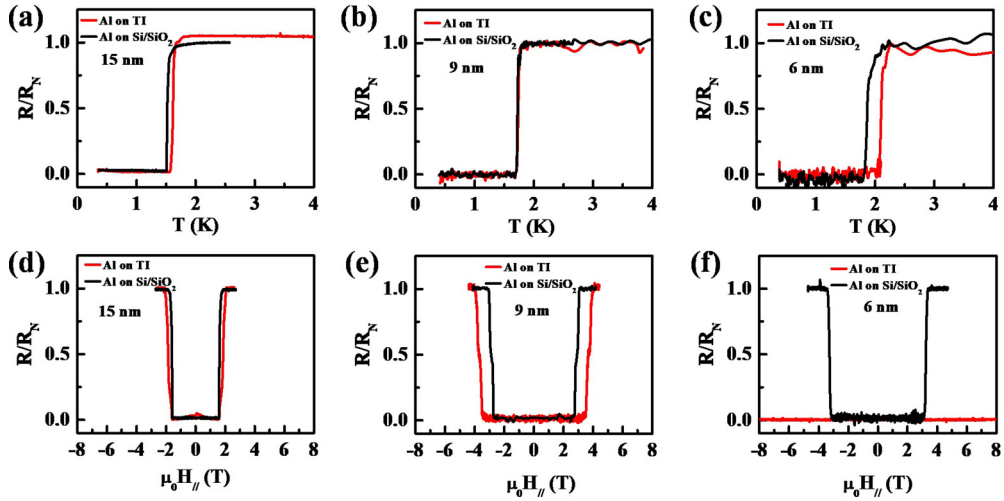

FIG. 2. Resistive transitions of Al films of different thicknesses on the TI and Si/SiO_2. (a)–(c) Normalized resistance versus temperature in zero magnetic field for three sets of Al films on the TI (red) and Si/SiO_2 (black). The Al thicknesses are 15, 9.0, and 6.0 nm, respectively. (d)–(f) Normalized resistance versus in-plane magnetic field at 0.40 K for the same three sets of Al films on the TI (red) and on Si/SiO_2 (black).

order to facilitate a more in-depth analysis of the increase of $H_{c||}$ of Al due to proximity coupling to the TI, the $R(H_{||})$ of the two 6-nm samples were measured at different temperatures between 0.40 K and their respective T_C's. The $R(H_{||})$ data are shown in Fig. S3 (Supplemental Material S3 [33]). Figure 3(b) shows the resulting $H_{c||}$ for the sample on Si/SiO_2 (black) and BSTS (red) at different temperatures. It is evident that $H_{c||}$ of the two 6-nm Al films not only differ in magnitude, but also exhibit qualitatively different T dependence.

For a superconducting film thinner than the penetration depth, a complete penetration of an in-plane magnetic field is allowed. Neglecting both orbital depairing and SO coupling, the zero-temperature H_c is given by the Pauli limit: $H_{c0} = H_p = \Delta_{00}/(\sqrt{g}\mu_B)$, where Δ_{00} is the energy gap at $T = 0$ and $H = 0$, μ_B is the Bohr magneton, and g is the Landé g factor [29]. The expression may be extended to finite temperatures to obtain the T dependence of $H_{c||}$:

$$H_{c\|}(T) = \Delta_0(T)/(\sqrt{g}\mu_B), \tag{1}$$

where $\Delta_0(T)$ is the zero-field superconducting gap at finite temperature. For superconductors in the BCS weak coupling limit, H_p can be rewritten as $H_p = 1.86T_C$ (teslas), assuming a g factor of 2. The black solid line in Fig. 4 is the theoretical curve calculated from Eq. (1) for the reference sample based on its zero-field T_C (1.87 K) and the BCS coupling constant. The T dependence of the experimental data is in good agreement with the theory, but the measured $H_{c||}(T)$ are consistently about 6% lower than the theoretical values, which is probably due to the small orbital depairing not accounted for in Eq. (1). In comparison, the experimental $H_{c||}(T)$ of the Al/BSTS sample is qualitatively different from Eq. (1), and the magnitudes are significantly larger, reaching 8 T at $T = 1.3$ K.

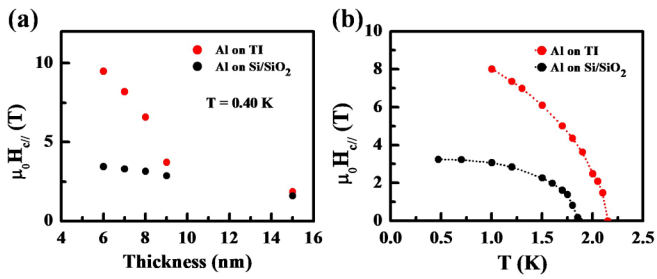

FIG. 3. Thickness and temperature dependences of the in-plane critical fields. (a) In-plane critical fields at $T = 0.40$ K for a set of Al films of varying thicknesses on BSTS (red circles) and reference samples on Si/SiO_2 (black circles). (b) In-plane critical fields of a pair of 6-nm Al films (red circles: on BSTS; black circles: on Si/SiO_2) as functions of temperature.

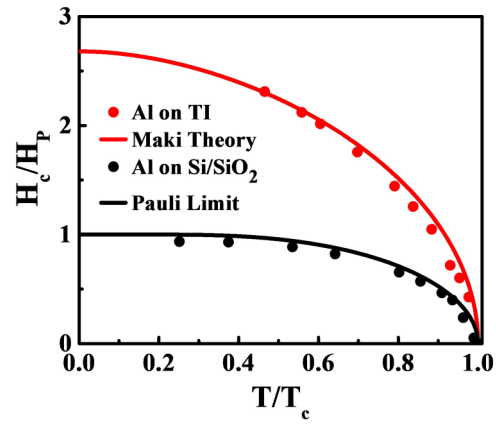

FIG. 4. Theoretical analysis of $H_{c||}(T)$ for 6-nm Al films. The symbols show the in-plane critical fields for the 6-nm Al films on BSTS (red circles) and Si/SiO_2 (black circles) normalized by their respective Pauli limit field (H_p). H_p is calculated from Δ_{00}, which is obtained via the BCS relation: $\Delta_{00} = 1.764\,k_BT_C$. From Fig. 2(c), for the Al on Si/SiO_2: $T_C = 1.87$ K, and for the Al on BSTS: $T_C = 2.15$ K. The Pauli limit and Maki theory curves are determined from Eqs. (1) and (2), respectively. A spin-orbit scattering rate of $b = (3.0 \pm 0.2)\Delta_{00}$ results from the Maki theory fitting.

III. THEORETICAL INTERPRETATION

SO interaction is known to preserve superconductivity in in-plane magnetic fields well in excess of the Pauli limit. The effective SO interaction can be intrinsic in origin, as in thin Pb films [36,37], or of the Ising type, as in mono- or few-layer transition-metal dichalcogenides [38–43], or extrinsic SO scattering by heavy element impurities [23,27]. The electronic structure of the surface states of the BSTS consists of a Dirac cone with strong spin-momentum locking [44,45]. The proximity of the Al film induces superconductivity into the electron gas. The Al should be considered a dirty superconductor with SO scattering centers. For a 3D *s*-SC this problem was studied by Maki [31], extending the theory of Abrikosov and Gor'kov [46] for magnetic impurities. A generalization to layered type II superconductors was carried out by Klemm *et al.* [47], who considered a model with translational invariance within the layers and interlayer tunneling of energy J. As a function of the field parallel to the layers and the inverse square of the hopping energy J, the model gives rise to a dimensional crossover from 3D to 2D. As a function of various model parameters (SO coupling, hopping J, and a diffusion constant across the layers), a rich variety of shapes of $H_c(T)$ dependences is obtained for in-plane fields. For relatively small interlayer tunneling, H_c shows a large enhancement above the Clogston-Chandrasekhar limit. For most of the materials the fluctuations induce a behavior like that of a highly anisotropic 3D superconductor.

In the present case the most important parameter is the SO scattering rate. The dependence on the thickness of the Al film arises (1) from the orbital effect, which is quenched in the thinner films, and (2) from the induced superconductivity into the TI and SO coupling into the nearest layers of Al (proximity effect and inverse proximity effect). Some of the effects discussed by Klemm *et al.* [47] with extreme anisotropy, such as normal cores of vortices effectively fitting in between the layers, do not apply to the present case. It is expected that $H_{c||}$ is determined by the combined effects of Pauli paramagnetism, disorder, and SO scattering, so that it suffices to use Maki's theory [31] to analyze our results. Quantitatively, the effect on the $H_c(T)$ is included in the Maki equation:

$$\ln\frac{T}{T_{c0}}=\psi\left(\frac{1}{2}\right)-\frac{\alpha_+}{2\gamma}\psi\left(\frac{1}{2}+\frac{\alpha_-}{2\pi T}\right)+\frac{\alpha_-}{2\gamma}\psi\left(\frac{1}{2}+\frac{\alpha_+}{2\pi T}\right), \quad (2)$$

where $\alpha_\pm = b \pm \gamma$, $b = \hbar/3\tau_{so}$, and $\gamma = \sqrt{b^2 - \mu_B^2 H_c^2}$. $b = \hbar/3\tau_{so}$ is the SO scattering rate regardless of its origin. $H_c(T)$ can be calculated from Eq. (2) by setting $\Delta = 0$. We point out that the H_c thus determined does not correspond to the superconducting-normal phase transition field when the phase transition is of first order, as in the limit of $b \to 0$ at low temperatures. Nevertheless, these two magnetic fields do coincide when the SC-normal phase transition is of second order, which is true for T close to T_{C0} in the case of negligible SO coupling ($b \to 0$), and for the entire temperature range below T_{C0} in the case of strong SO scattering ($b \gg \mu_B H$). To avoid this complication, for the reference sample, we use Eq. (1) to describe its $H_{c||}(T)$ for all temperatures. For the Al/BSTS sample, Eq. (2) is applicable: The $H_{c||}(T)$ data, normalized by its $T_{C0} = 2.15$ K and the corresponding H_p, are compared to Eq. (2). In the calculation of the theoretical curves, the orbital depairing is neglected based on its minimal effect on the reference sample. That leaves b as the *only* adjustable parameter in the calculation of $H_c(T)$. In Supplemental Material S4 [33], we plot five theoretical curves of varying b from $2.6\Delta_{00}$ to $3.4\Delta_{00}$. Among them, the curve with $b = 3.0\,\Delta_{00}$ is deemed to provide the best agreement with the extrapolation of the experimental $H_{c||}$ to low T, shown as the red solid curve in Fig. 4. The comparison thus results in H_{c0} of $2.7H_p$ (9.3 T) and SO scattering rate of $(3.0 \pm 0.2)\Delta_{00}$. Two points are worth noting here: (i) The large magnitude of the induced b in the Al constitutes direct evidence for strong proximity coupling between the Al and the TI. (ii) The giant enhancement of $H_{c||}$ for the thin Al on the TI further implies that the proximity coupling is predominantly between the Al and the surface state of the TI. There is minimal proximity effect between the Al and the (insulating) bulk of the TI, because otherwise the effective superconducting thickness of the bilayer would be significantly increased and $H_{c||}$ enhancement suppressed due to orbital depairing. We also point out that although in principle the SO scattering rate in the Al film could be determined directly from weak (anti)localization measurements [48], the multiple channel parallel conduction from the top and bottom surfaces of the TI with the Al film renders the Hikami-Larkin-Nagaoka analysis highly complex and probably unreliable [34].

IV. CONCLUSIONS

In summary, we have probed the proximity coupling between a 3D strong TI and a conventional *s*-wave superconductor with minimal spin-orbit coupling, via measurement of the enhancement of the in-plane critical field of the thin *s*-SC. The $H_{c||}$ of a 6-nm-thick Al film deposited on BSTS is about three times that of the simultaneously deposited Al film on Si/SiO_2. The enhanced $H_{c||}$ is well described by the Maki theory, with significant SO scattering in the Al due to proximity coupling to the BSTS. The results indicate an Al/BSTS interface of high electrical transparency. The high interfacial transparency was obtained despite a brief exposure of the exfoliated BSTS to ambient air before the deposition of Al, which suggests that exposure to solvents and/or high-energy electrons is more damaging to the *s*-SC/TI interface. Our work reveals that direct shadowed deposition of the *s*-SC on the TI, rather than conventional schemes based on electron-beam lithography, is more conducive to producing SC/TI devices for MZM generation and manipulation.

ACKNOWLEDGMENTS

We thank S. von Molnár for helpful discussions. The work at FSU was supported by DARPA TEE Program (Cooperative Agreement No. D18AC00010) and NSF Grant No. DMR-1905843. The work at IOP-CAS was supported by the National Key Research and Development Program (Project No. 2016YFA0300600), the National Natural Science Foundation of China (Project No. 61425015), and the Strategic Priority Research Program of Chinese Academy of Sciences (Project No. XDB28000000).

[1] A. Kitaev, Ann. Phys. **303**, 2 (2003).

[2] C. Nayak, S. H. Simon, A. Stern, M. Freedman, and S. Das Sarma, Rev. Mod. Phys. **80**, 1083 (2008).

[3] Y. Maeno, H. Hashimoto, K. Yoshida, S. Nishizaki, T. Fujita, J. G. Bednorz, and F. Lichtenberg, Nature **372**, 532 (1994).

[4] Y. S. Hor, A. J. Williams, J. G. Checkelsky, P. Roushan, J. Seo, Q. Xu, H. W. Zandbergen, A. Yazdani, N. P. Ong, and R. J. Cava, Phys. Rev. Lett. **104**, 057001 (2010).

[5] D. Wang, L. Kong, P. Fan, H. Chen, S. Zhu, W. Liu, L. Cao, Y. Sun, S. Du, J. Schneeloch, R. Zhong, G. Gu, L. Fu, H. Ding, and H. J. Gao, Science **362**, 333 (2018).

[6] S. Zhu, L. Kong, L. Cao, H. Chen, M. Papaj, S. Du, Y. Xing, W. Liu, D. Wang, C. Shen, F. Yang, J. Schneeloch, R. Zhong, G. Gu, L. Fu, Y. Y. Zhang, H. Ding, and H. J. Gao, Science **367**, 189 (2020).

[7] R. M. Lutchyn, J. D. Sau, and S. Das Sarma, Phys. Rev. Lett. **105**, 077001 (2010).

[8] L. Fu and C. L. Kane, Phys. Rev. Lett. **100**, 096407 (2008).

[9] V. Mourik, K. Zuo, S. M. Frolov, S. R. Plissard, E. P. A. M. Bakkers, and L. P. Kouwenhoven, Science **336**, 1003 (2012).

[10] M. T. Deng, S. Vaitiekėnas, E. B. Hansen, J. Danon, M. Leijnse, K. Flensberg, J. Nygård, P. Krogstrup, and C. M. Marcus, Science **354**, 1557 (2016).

[11] H.-H. Sun, K.-W. Zhang, L.-H. Hu, C. Li, G.-Y. Wang, H. Y. Ma, Z. A. Xu, C. L. Gao, D. D. Guan, Y. Y. Li, C. Liu, D. Qian, Y. Zhou, L. Fu, S. C. Li, F. C. Zhang, and J. F. Jia, Phys. Rev. Lett. **116**, 257003 (2016).

[12] L. A. Jauregui, M. Kayyalha, A. Kazakov, I. Miotkowski, L. P. Rokhinson, and Y. P. Chen, Appl. Phys. Lett. **112**, 093105 (2018).

[13] G. Yang, Z. Lyu, J. Wang, J. Ying, X. Zhang, J. Shen, G. Liu, J. Fan, Z. Ji, X. Jing, F. Qu, and L. Lu, Phys. Rev. B **100**, 180501(R) (2019).

[14] Y. Pang, J. Wang, Z. Lyu, G. Yang, J. Fan, G. Liu, Z. Ji, X. Jing, C. Yang, and L. Lu, Chin. Phys. B **25**, 117402 (2016).

[15] R. S. Deacon, J. Wiedenmann, E. Bocquillon, F. Domínguez, T. M. Klapwijk, P. Leubner, C. Brüne, E. M. Hankiewicz, S. Tarucha, K. Ishibashi, H. Buhmann, and L. W. Molenkamp, Phys. Rev. X **7**, 021011 (2017).

[16] J. R. Williams, A. J. Bestwick, P. Gallagher, S. S. Hong, Y. Cui, A. S. Bleich, J. G. Analytis, I. R. Fisher, and D. Goldhaber-Gordon, Phys. Rev. Lett. **109**, 056803 (2012).

[17] M. Kayyalha, M. Kargarian, A. Kazakov, I. Miotkowski, V. M. Galitski, V. M. Yakovenko, L. P. Rokhinson, and Y. P. Chen, Phys. Rev. Lett. **122**, 047003 (2019).

[18] B. Sacépé, J. B. Oostinga, J. Li, A. Ubaldini, N. J. G. Couto, E. Giannini, and A. F. Morpurgo, Nat. Commun. **2**, 575 (2011).

[19] M. Veldhorst, M. Snelder, M. Hoek, T. Gang, V. K. Guduru, X. L. Wang, U. Zeitler, W. G. van der Wiel, A. A. Golubov, H. Hilgenkamp, and A. Brinkman, Nat. Mater. **11**, 417 (2012).

[20] S. Cho, B. Dellabetta, A. Yang, J. Schneeloch, Z. Xu, T. Valla, G. Gu, M. J. Gilbert, and N. Mason, Nat. Commun. **4**, 1689 (2013).

[21] C. Kurter, A. D. K. Finck, Y. S. Hor, and D. J. Van Harlingen, Nat. Commun. **6**, 7130 (2015).

[22] F. Domínguez, O. Kashuba, E. Bocquillon, J. Wiedenmann, R. S. Deacon, T. M. Klapwijk, G. Platero, L. W. Molenkamp, B. Trauzettel, and E. M. Hankiewicz, Phys. Rev. B **95**, 195430 (2017).

[23] P. M. Tedrow and R. Meservey, Phys. Rev. Lett. **43**, 384 (1979).

[24] P. M. Tedrow and R. Meservey, Phys. Rev. B **25**, 171 (1982).

[25] X. S. Wu, P. W. Adams, and G. Catelani, Phys. Rev. Lett. **95**, 167001 (2005).

[26] V. Y. Butko, P. W. Adams, and I. L. Aleiner, Phys. Rev. Lett. **82**, 4284 (1999).

[27] P. W. Adams, Phys. Rev. Lett. **92**, 067003 (2004).

[28] P. Fulde, Adv. Phys. **22**, 667 (1973).

[29] A. M. Clogston, Phys. Rev. Lett. **9**, 266 (1962).

[30] B. S. Chandrasekhar, Appl. Phys. Lett. **1**, 7 (1962).

[31] K. Maki, Phys. Rev. **148**, 362 (1966).

[32] K. Aoi, R. Meservey, and P. M. Tedrow, Phys. Rev. B **7**, 554 (1973).

[33] See Supplemental Material at http://link.aps.org/supplemental/10.1103/PhysRevB.102.144518 for material preparation, device fabrication, electrical measurements, resistance of a reference sample of blank BSTS flake, aligning the film plane with applied magnetic field, magnetoresistance of the 6-nm Al device at different temperatures, Maki fittings of the in-plane critical fields for the 6-nm Al film on BSTS; also see Refs. [34,35].

[34] L. Yu, L. Hu, J. L. Barreda, T. Guan, X. He, K. Wu, Y. Li, and P. Xiong, Phys. Rev. Lett. **124**, 126601 (2020).

[35] J. S. Parker, Investigation of materials with high spin polarization via spin polarized transport, Ph.D. dissertation, Florida State University, 2003.

[36] H. J. Gardner, A. Kumar, L. Yu, P. Xiong, M. P. Warusawithana, L. Wang, O. Vafek, and D. G. Schlom, Nat. Phys. **7**, 895 (2011).

[37] H. Nam, H. Chen, T. Liu, J. Kim, C. Zhang, J. Yong, T. R. Lemberger, P. A. Kratz, J. R. Kirtley, K. Moler, P. W. Adams, A. H. MacDonald, and C. K. Shih, Proc. Natl. Acad. Sci. USA **113**, 10513 (2016).

[38] J. M. Lu, O. Zheliuk, I. Leermakers, N. F. Q. Yuan, U. Zeitler, K. T. Law, and J. T. Ye, Science **350**, 1353 (2015).

[39] Y. Saito, Y. Nakamura, M. S. Bahramy, Y. Kohama, J. Ye, Y. Kasahara, Y. Nakagawa, M. Onga, M. Tokunaga, T. Nojima, Y. Yanase, and Y. Iwasa, Nat. Phys. **12**, 144 (2016).

[40] Y. Saito, T. Nojima, and I. Yoshihiro, Nat. Rev. Mater. **2**, 16094 (2017).

[41] X. Xi, Z. Wang, W. Zhao, J.-H. Park, K. T. Law, H. Berger, L. Forró, J. Shan, and K. F. Mak, Nat. Phys. **12**, 139 (2016).

[42] Y. Xing, K. Zhao, P. Shan, F. Zheng, Y. Zhang, H. L. Fu, Y. Liu, M. Tian, C. Xi, H. Liu, J. Feng, X. Lin, S. H. Ji, X. Chen, Q. K. Xue, and J. Wang, Nano Lett. **17**, 6802 (2017).

[43] S. C. Barrera, M. R. Sinko, D. P. Gopalan, N. Sivadas, K. L. Seyler, K. Watanabe, T. Taniguchi, A. W. Tsen, X. Xu, D. Xiao, and B. M. Hunt, Nat. Commun. **9**, 1427 (2018).

[44] T. Arakane, T. Sato, S. Souma, K. Kosaka, K. Nakayama, M. Komatsu, T. Takahashi, Z. Ren, K. Segawa, and Y. Ando, Nat. Commun. **3**, 636 (2018).

[45] T. F. Kasalak, A. Babanli, S. Çakmak, and İ. Yücel, Optoelectron. Adv. Mater. Rapid Commun. **10**, 391 (2016).

[46] A. A. Abrikosov and L. P. Gor'kov, Zh. Eksp. Teor. Fiz. **39**, 1781 (1960) [Sov. Phys. JETP **12**, 1243 (1961)].

[47] R. A. Klemm, A. Luther, and M. R. Beasley, Phys. Rev. B **12**, 877 (1975).

[48] G. Bergmann, Phys. Rep. **107**, 1 (1984).